



Research Article

The Research on Risk Distribution and Evolution of Deep Foundation Pit Construction Adjacent to Existing Tunnels Based on Complex Network

Jie Jiang ^{1,2,3}, Guangyang Liu ^{1,2,3}, Xi Huang^{1,2,3} and Xiaoduo Ou^{1,2,3}

¹College of Civil Engineering and Architecture, Guangxi University, Nanning 530004, China

²Key Laboratory of Disaster Prevention and Structural Safety of Ministry of Education, Guangxi University, Nanning 530004, China

³Guangxi Key Laboratory of Disaster Prevention and Engineering Safety, Guangxi University, Nanning 530004, China

Correspondence should be addressed to Guangyang Liu; 552411662@qq.com

Received 4 April 2022; Revised 6 July 2022; Accepted 27 July 2022; Published 14 September 2022

Academic Editor: Biao Li

Copyright © 2022 Jie Jiang et al. This is an open access article distributed under the Creative Commons Attribution License, which permits unrestricted use, distribution, and reproduction in any medium, provided the original work is properly cited.

The construction of deep foundation pits adjacent to existing subway tunnels faces enormous challenges, and once a safety accident occurs, there are often mass injuries that cause substantial economic losses. However, there are many shortcomings and defects in the traditional methods of assessing the safety of the pit itself and the existing tunnel in the construction of the deep foundation pit adjacent to existing tunnels. This study establishes an optimized complex network-based dynamic risk assessment model to dynamically assess the overall risk of deep foundation pits in adjacent existing tunnels systematically, solving the challenges of inaccurate risk assessment and inaccurate description of correlations between nonstationary time series data. In this study, we first divide the monitoring data into time windows and describe the correlation between nonstationary time-series monitoring data within each window based on the MF-DCCA method and the threshold method, and establish the adjacency matrix to prepare for the establishment of an optimized complex network model. Secondly, based on the adjacency matrix, a complex network model under different time windows is constructed, and risk assessment indexes are established through the topological parameters of the complex network model to explore the evolution of risk in time and space, so as to realize the risk distribution and quantitative evolution assessment of the system which is deep foundation pit adjacent to existing subway tunnels. Finally, the proposed method is tested by taking the Nanning underground comprehensive utilization project as an example. The results show that this method can quantify the risk of the construction of deep foundation pits adjacent to existing tunnels more effectively than the traditional method to describe the evolution law better. It has important guiding significance for strengthening the safety risk monitoring and safety management of the construction system of deep foundation pits adjacent to existing tunnels.

1. Introduction

To facilitate people to travel, many buildings are often built near existing subway tunnels [1]. Deep foundation excavation will not only cause deformation or differential settlement of the surrounding existing buildings (structures). However, it will also interact with the geotechnical body around existing subway tunnel, causing longitudinal settlement and lateral deformation of the tunnel structure, ultimately affecting the force conditions and service functions of the tunnel [2, 3]. Therefore, the complex conditions

of the adjacent existing tunnel caused considerable construction difficulties for the deep foundation excavation [4]. More and more outstanding scholars have studied the safety of geotechnical bodies around existing underground structures. Li et al. [5] analyzed the microseismic b -value and its variation with time by establishing two microseismic monitoring systems, which provided a reference for early warning of large deformation of underground plant cavities. Lai et al. [6] illustrate the value of multi-parameter measurement campaigns in assessing the impact of disturbances caused by new excavations on pre-existing underground

structures, based on a practical case of gold mining. These examples indicate that the safety assessment of the surrounding geotechnical body of existing underground structures has become a hot topic of research today, and the deep foundation pit excavation adjacent to existing tunnels is a typical one.

The construction system of deep foundation pits adjacent to existing tunnels has the following typical characteristics: First, the complexity of the interaction between the pit and the existing tunnel; second, the high demand for deformation control of pits and existing tunnels; third, the high-risk nature of construction. In order to evaluate the safety of deep foundation construction in such complex working conditions, many scholars have conducted a lot of research using many methods. Zheng et al. [7] used the finite element method to parametrically analyze the deformation influence law of existing underpass tunnels outside the pit, and divided the existing tunnel deformation zone under different enclosure structure deformation modes and maximum horizontal displacement conditions; Jiang and Zhang [8] summarized a method to calculate the displacement of existing subway tunnels adjacent to the foundation excavation based on existing research results; Xu et al. [9] used ABAQUS numerical simulation analysis and simplified canonical corner point method, respectively, to compare and analyze the impact of foundation excavation on existing underlying road tunnels. Existing research methods that demonstrate the effect of excavation on existing metro deformation through mechanical theory and numerical analysis do not provide a basis for dynamic decision-making in construction projects. In traditional dynamic construction risk assessment methods, fuzzy theory-based assessment methods such as the fuzzy integrated judgment method are too subjective in assessment [10–12]. The threshold method based on the comparison of monitoring data and design criteria (or design requirements) has the same unavoidable limitations [13, 14]: First, the monitoring point in different times and spaces under the risk threshold is not the same, only set a unified risk domain value is prone to cause misjudgment in risk control [15]. Second, a simple threshold comparison can only provide the level of risk at a single point, but cannot provide the overall risk and quantify the process of risk evolution at the construction site. In addition, scholars have tried to use complex network theory for foundation pit construction risk assessment. For example, Zhou et al. [16] established a complex network model of the deep foundation pit surface system based on the complex network theory, based on the monitoring data of the deep foundation pit surface system, and quantitatively assessed the risk of the deep foundation pit system and its time and space evolution, but its use of Pearson correlation coefficient could not effectively express the nonlinear correlation between nonstationary time series.

In summary, the shortcoming of the abovementioned study is that the current approach cannot dynamically assess the overall risk of deep foundation pits in adjacent existing

tunnels from a systematic perspective [17]. In addition, the construction of deep foundation pits adjacent to existing tunnels is very complex and contains many elements with strong nonlinear coupling between them, and the dynamic time and space evolution law of the system is also nonlinear, which cannot be described by general numerical simulation methods and analytical methods. Therefore, it is of great practical significance to explore an effective method to dynamically assess the risk of the construction system of deep foundation pits adjacent to existing tunnels from the system perspective.

In this study, the MF-DCCA method was introduced into the risk assessment of the deep foundation pit system adjacent to the existing tunnel for the first time. At present, the MF-DCCA method has been widely used in foreign exchange, stocks, crude oil, and other fields [18–20]. The MF-DCCA method can effectively and quantitatively describe the nonlinear correlation between unstable sequences [21], and it can be used to capture the nonlinear correlation of elements in the construction system of deep foundation pits adjacent to existing tunnels, which is of great significance for optimizing complex networks. Therefore, based on the complex network theory, this study takes the displacement system of the deep foundation pit adjacent to the existing tunnel as the object and establishes an optimized spatiotemporal complex network model of the construction system of deep foundation pits adjacent to existing tunnels. And quantitatively and dynamically assess the risk and evolution of the construction system of deep foundation pits adjacent to existing tunnels from the perspective of time and space, providing a new method for the risk assessment and construction guidance of the construction system of deep foundation pits adjacent to existing tunnels. Taking the underground space utilization project of Nanning Rail Transit Line 5 from Guangxi University Station to Guangxi Institute of Finance and Economics as an example, the effectiveness and feasibility of the method are verified.

This study is organized as follows: Section 2 briefly introduces the theoretical basis of the new method proposed in this study. Section 3 outlines the framework of the risk assessment process using the method proposed in this study. Section 4 uses the method proposed in this study to study an underground space utilization project in Nanning to verify its feasibility. Section 5 comprehensively discusses the validity and accuracy of the method proposed in this study in risk assessment of deep foundation pits adjacent to existing tunnels. Finally, Section 6 summarizes the research work of this study.

2. Methodology

2.1. Correlation Coefficient of Different Monitoring Points

2.1.1. DCCA Method. The cross-correlation coefficient DCCA is used to qualitatively test the degree of cross-correlation between two nonstationary time series [22–24]. Suppose there are two time series $x(t)$ and $y(t)$, $t = 1, 2, \dots, N$, the coefficient is defined as:

$$\rho_{\text{DCCA}} = \frac{F_{\text{DCCA}}^2(s)}{F_{\text{DF,AX}(t)}(s)F_{\text{DF,AY}(t)}(s)}, \quad (1)$$

$$X(t) = \sum_{k=1}^t [x(k) - \bar{x}], \quad (2)$$

where $F_{\text{DFA},X(t)}(s)$ and $F_{\text{DFA},Y(t)}(s)$ are detrended variances of partial sums $X(t)$ and $Y(t)$, respectively, [25, 26]:

$$F_{\text{DFA},X(t)}^2(s) = \frac{\sum_{j=1}^{T-s+1} \left[(s-1)^{-1} \sum_{k=j}^{j+s-1} (X(k) - \bar{X}(k, j))^2 \right]}{T-s}, \quad (3)$$

$$F_{\text{DFA},Y,t}^2(s) = \frac{\sum_{j=1}^{T-s+1} \left[(s-1)^{-1} \sum_{k=j}^{j+s-1} (Y(k) - \bar{Y}(k, j))^2 \right]}{T-s}, \quad (4)$$

where \bar{X}, k, j can be obtained by establishing a linear fit of the time trend over the range j to $j+s-1$ for each interval. $F_{\text{DCCA}}^2(s)$ is a detrended covariance between partial sums $\{X_i\}$ and $\{Y_i\}$ for a window size s :

$$F_{\text{DCCA}}^2(s) = \frac{\sum_{j=1}^{T-s+1} f_{\text{DCCA}}^2(s, j)}{T-s}, \quad (5)$$

$$f_{\text{DCCA}}^2(s, j) = \frac{\sum_{k=j}^{j+s-1} (X(k) - \bar{X}(k, j))(Y(k) - \bar{Y}(k, j))}{s-1}. \quad (6)$$

The study by Podobnik et al. [27] shows that the value range of ρ_{DCCA} is $-1 \leq \rho_{\text{DCCA}} \leq 1$, when $\rho_{\text{DCCA}} = 1$, it represents a perfectly correlated series, when $\rho_{\text{DCCA}} = 0$, it means an uncorrelated process, and when $\rho_{\text{DCCA}} = -1$, it means They are completely anticorrelated series.

2.1.2. Cross-Correlation Test. The cross-correlation statistic proposed by Podobnik [26] can be used to qualitatively analyze whether two time series have cross-correlation. Assume there are two time series $x(t)$ and $y(t)$, $t = 1, 2, \dots, N$, The cross-correlation test statistic $Q_{cc}(m)$ is defined as:

$$Q_{cc}(m) = N^2 \sum_{i=1}^m \frac{X(i)^2}{N-i}, \quad (7)$$

where the cross-correlation function $X(i)$ is defined as:

$$X(i) = \frac{\sum_{k=i+1}^N x(t)y(t-i)}{\sqrt{\sum_{t=1}^N x(t)^2 \sum_{t=1}^N y(t)^2}}. \quad (8)$$

The null hypothesis for the $Q_{cc}(m)$ statistic test is that if the cross-correlation statistic $Q_{cc}(m)$ of two columns of time series with m degrees of freedom follows the χ^2 distribution (critical value), then the two time series do not have cross-correlation.

2.2. MF-DCCA Method. The MF-DCCA [21] method can effectively eliminate the influence of local trends on the time series scale and can observe the multifractality of the time series at different time scales. It also needs to construct two new time series $X(t)$ and $Y(t)$. Divide the newly constructed single time series into $N_s = \text{int}(N/s)$ time windows of length s .

$$X(t) = \sum_{k=1}^i [x(k) - \bar{x}], \quad (9)$$

$$Y(t) = \sum_{k=1}^i [y(k) - \bar{y}], \quad (10)$$

$$X_\lambda(i) = a_k i^m + \dots + a_1 i + a_0, \quad (11)$$

$$Y_\lambda(i) = b_k i^m + \dots + b_1 i + b_0. \quad (12)$$

The local covariance function $F^2(s, \lambda)$ is obtained by subtracting the local trend function $X_\lambda(i)$ and $Y_\lambda(i)$ from the original time series to eliminate the trend for each time window.

$$F^2(s, \lambda) = \frac{1}{s} \sum_{i=1}^s \{X[N - (\lambda - N_s)s + i] - X_\lambda(i)\} \quad (13)$$

$$\times \{Y[N - (\lambda - N_s)s + i] - Y_\lambda(i)\},$$

$$F_q(s) = \left\{ (2N_s)^{-1} \sum_{\lambda=1}^{2N} [F^2(s, \lambda)] \right\}^{1/q}, \quad q \neq 0, \quad (14)$$

where $F_q(s)$ is the q order fluctuation function, which can be obtained by averaging the local covariance over $2N_s$ windows. If there is a power-law relationship between $F_q(s)$ and the scalar scale s , the scalar relationship between them is given by formula (15):

$$F_q(s) \sim s^{H_{xy}(q)}, \quad (15)$$

where $H_{xy}(q)$ is the generalized Hurst index, and when $q=2$, the MF-DCCA method degenerates to the DCCA method, which is sufficient for assessing the cross-correlation between two nonstationary time series.

2.3. Determination of the Optimal Threshold and Construction of Complex Networks. The first principle of threshold selection is to ensure the assumed nature of the constructed complex network, i.e., the scale-free and small-world nature that a general complex network would have. The scale-free nature requires that the threshold must be set so that the edge (degree) distribution of the complex network model obeys a power-law distribution [28, 29], that is, the following relationship:

$$P(k) \sim k^{-a}, \quad (16)$$

where $P(k)$ represents the ratio of the number of nodes with k connected edges to the number of all nodes in the network and α represents the power-law exponent.

In order to avoid the influence of the number of nodes on the threshold value of the network model, construct $(C_{\text{ran}})^{-1}C$ and $(L_{\text{ran}})^{-1}L$, respectively. Take the ratio S of the two indicators to construct the small-world indicator, and the formula is as follows:

$$(C_{\text{ran}})^{-1}C = \left(\frac{\bar{K}}{N}\right)^{-1} C = (\bar{K})^{-1}CN, \quad (17)$$

$$(L_{\text{ran}})^{-1}L = \left(\frac{\ln N}{\ln \bar{K}}\right)^{-1} L = (\ln N)^{-1}L \ln K, \quad (18)$$

$$S = \left(\frac{L}{L_{\text{ran}}}\right)^{-1} \frac{C}{C_{\text{ran}}}, \quad (19)$$

where C is the feature clustering coefficient in the complex network model, L is the length of the feature path, N is the number of nodes in the network, and \bar{K} is the average of all edges in the network. When the threshold-optimized network model satisfies the small-world index $S \gg 1$, it is used as the lower limit of the threshold value [30], and the degree distribution of the network model also needs to conform to the power-law distribution, that is, there is a power exponent α .

The second principle of threshold selection is to ensure the connectivity of the network. There are no isolated nodes in the network. Otherwise, the quantification of the importance of isolated nodes will be invalid during model risk assessment [31]. At the same time, random small-world networks are connected in such a way that any node is randomly connected to other nodes in the network with a probability p . When the minimum connectivity probability is 0.1, the total number of edges in the existing network is $K^* \approx 0.1K$, where K is the total number of edges in the original fully connected network.

To sum up, the selection range of the threshold should first ensure that there are no isolated nodes in the network, and the upper and lower limits of the threshold should be selected to ensure that $S \gg 1$ and $K^* \geq 0.1K$, and to ensure that the power exponent α exists. Finally, the optimal threshold can be selected as the threshold with the largest small-world index.

2.4. Risk Assessment of Complex Networks. Topological parameters that describe network structure and node characteristics are the main means to quantitatively assess complex network models. In the process of complex network research, many classical topology parameters are constructed to describe the structural characteristics of different complex network models and establish system model risk assessment indicators. From the perspectives of time and space of the construction system of deep foundation pits adjacent to existing tunnels, the assessment of the spatial distribution of risks and evolution of construction risks of the construction system of deep foundation pits adjacent to existing tunnels are carried out.

2.4.1. Time Risk Evolution Based on Network Entropy. From the time perspective of the construction system of deep foundation pits adjacent to existing tunnels, it is necessary to construct the overall risk evolution assessment index of the system model. The network structure entropy is generated based on the degree of nodes. As a measure of the disorder degree of a complex system, it is an important indicator to reflect the risk characteristics and evolution of the network model. [32–34], This research is mainly based on the quantification of the structural entropy of the network model to establish the overall risk index of the construction system of deep foundation pits adjacent to existing tunnels and to observe the dynamic characteristics of the risk by calculating the entropy.

$$E = - \sum_{i=1}^N \frac{k_i}{\sum_{i=1}^N k_i} \ln \left(\frac{k_i}{\sum_{i=1}^N k_i} \right), \quad (20)$$

where E is the network entropy and k_i is the total number of edges of the node i . In order to exclude the influence of the number of different nodes N on the entropy value E , the normalized value of the entropy of the network structure is used as the absolute risk value of the system network model, and also as the absolute risk value R of the construction system of deep foundation pits adjacent to existing tunnels represented by this network model:

$$R = \bar{E} = \frac{E - E_{\min}}{E_{\max} - E_{\min}}, \quad (21)$$

where \bar{E} is the normalized network entropy of the network, obviously, $0 \leq R = \bar{E} \leq 1$.

2.4.2. Spatial Risk Distribution Based on Network Structure. Identifying the nodes that have the most significant impact on system security is crucial to exploring the spatial distribution of risks. The importance of a single node is directly related to the degree of damage to the system security caused by removing the node. For a certain safety factor X_i of the safety system, the ability to complete the specified contribution to the safety function of the system as a whole can be represented by its safety degree $P(x_i)$. The topology parameters of complex networks are often used to assess the importance of nodes in complex networks, such as betweenness centrality. The node with the largest betweenness centrality has the greatest impact on the security of the topology [35]. Therefore, this study uses the betweenness centrality index to quantify the importance of nodes in the model. The greater the betweenness of the node X_i , the greater its security $P(x_i)$, and the greater the contribution to the system risk. The location of high-safety nodes can reflect the risk distribution of the construction system of deep foundation pits adjacent to existing tunnels.

$$P(x_i) = C_B = \frac{2}{(N-1)(N-2)} \sum_{s \neq i \neq t} \frac{g_{st}(i)}{g_{st}}, \quad (22)$$

where g_{st} is the number of all shortest paths from node s to node t , $g_{st}(i)$ is the number of paths through node i among the shortest paths from node s to node t . $2/(N-1)(N-2)$ is the normalization factor. The Max-Min deviation of each node's betweenness $P(x_i)$ is normalized to the risk value of a node.

$$R(x_i) = \frac{P(x_i) - \min_{1 \leq j \leq n} P(x_j)}{\max_{1 \leq j \leq n} P(x_j) - \min_{1 \leq j \leq n} P(x_j)}, \quad (23)$$

where $\min_{1 \leq j \leq n} P(x_j)$ and $\max_{1 \leq j \leq n} P(x_j)$, respectively, represent the minimum and maximum values of node security in a network model with n nodes. The value of $R(x_i)$ is between $[0, 1]$.

3. Assessment Framework for Construction Risk Evolution

The framework of this assessment includes four key components, the specific steps are as follows (Figure 1):

- (1) Data collection and correlation analysis: Collect and process displacement monitoring data at different points in foundation pits and existing tunnels, which are typical nonstationary time series. In this study, a moving time observation window is set up on the time axis, and the unstable time series data are divided by the time observation window. Based on the nonstationary time series data in each time observation window, the complex network model of the deep foundation pit settlement system in the current time window is generated, and the network models under different time windows are formed. However, the correlation analysis of nonstationary time series data is a prerequisite for constructing a correlation matrix and establishing a complex network. Therefore, it is necessary to use the MF-DCCA method to analyze the nonstationary time series data of monitoring points around the foundation pit and existing tunnels, and then convert the time series data into a correlation matrix.
- (2) Construction and optimization of complex networks: The monitoring points in the construction system of deep foundation pits adjacent to existing tunnels are uniformly regarded as network nodes. Since there is a tendency for monitoring points in the system to respond to each other and change together, the interrelationship between monitoring points is quantitatively described to form the correlation between the nodes in a complex network system with connected edges. These correlation characteristics need to be obtained from the nonstationary time series data monitored by each measuring point and are represented by the weighted and undirected edges between the nodes. Firstly, the original correlation matrix is constructed based on the nonlinear cross-correlation between the displacement settlement data of different monitoring points in each window. Then, the optimal threshold value for each

window is solved, the complex network is constructed using the edge correlation coefficient threshold method, and finally, a series of network models with unique topological characteristics are obtained.

- (3) Risk Evolution Assessment: By studying the complex network model with different time windows, analyzing the Wu structure entropy value and relative risk value, then simulating and quantifying the evolution of the risk of the deep foundation pit displacement system with the construction process, and finding out the time windows of high risk. Then, the risk value of each monitoring point is obtained by comparing and studying the betweenness centrality of each monitoring point in a certain high-risk window, and then the spatial variation of the risk of the complex network model under this time window is obtained.
- (4) Comparative analysis: Based on the "Weekly Security Inspection Report" of accidents occurring in actual construction, the assessment results are compared and analyzed with the events and locations of actual accidents to verify the effectiveness of the risk assessment method proposed in this study.

4. Case Study

4.1. Project Overview. This study takes the underground space utilization project from Guangxi University Station to Guangxi Finance and Economics College of Nanning Metro Line 5 as the case object of the study. The project is laid along the east-west direction of Ming Xiu West Road, starting near the intersection of Ming Xiu West Road and HuoJu Branch Road, and finally near the entrance of the School of Finance and Economics. It will be built as an underground commercial street with an underground multi-span single-story rectangular structure. The total length of the main structure is 811.2 m, the standard width of the main foundation pit is 28.8 m, the depth of the foundation pit is 8.6–10.5 m, and the total construction area is 36000 m². The main foundation pit of the project adopts the support form of bored cast-in-place piles and internal supports. The foundation pit support system uses two supports, as shown in Figure 2 for the deep foundation pit support structure. Set up multiple entrances and exits and ancillary facilities such as wind pavilions. The project is surrounded by extremely complex facilities and is located above the interval of Guangxi Daxi Station-Xiuling Road Station of Metro Line 5. The vertical clear distance is 5 m–8.7 m, and the soil at the bottom of the pit needs to be reinforced before excavation to reduce pit uplift and tunnel uplift, and to strengthen monitoring in the pit and tunnel. In addition, there are buildings such as Nanning Vocational and Technical College, Guangxi Finance and Economics College Teaching Building, and Construction Bank Ming Xiu West Road Branch Office adjacent to the projected pit, as shown in Figure 3. Quaternary soil layers are overlaid on the site, from top to bottom: plain fill, hard plastic silty clay, plastic silty clay, soft plastic silty clay, fine sand, pebbles, and

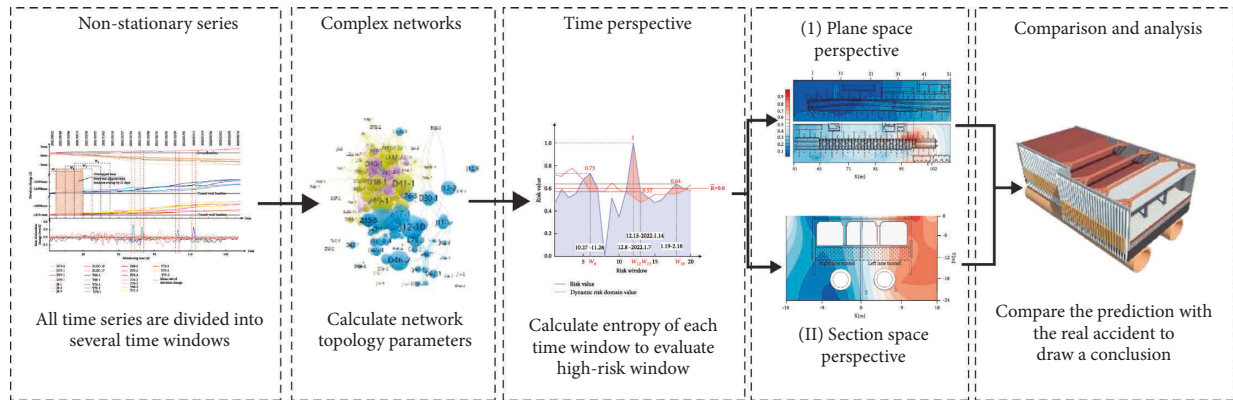


FIGURE 1: Flow chart for quantifying the risk evolution of deep foundation pits adjacent to existing tunnels.

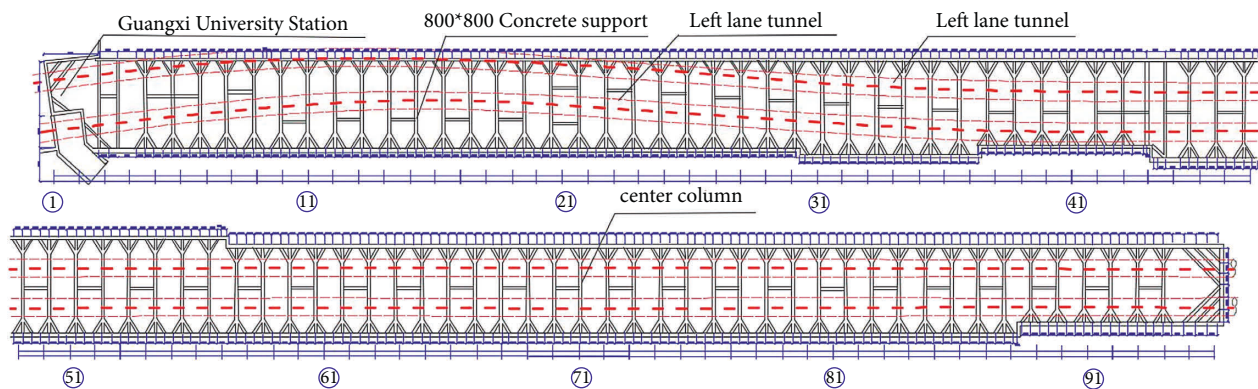


FIGURE 2: Supporting structure of deep foundation pit adjacent to existing tunnel Guangxi University of Finance and Economics.

Paleogene mudstone. The base plate of the project is located in the powder clay, plastic powder clay, soft plastic powder clay, and fine sand layer, and the groundwater is mainly pore diving, endowed with a compressive round gravel layer, the geological and enclosure structure profile is shown in Figure 4. The excavation of the foundation pit strictly implements the principles of longitudinal segmentation, transverse segmentation, and vertical stratification, the longitudinal direction is no more than 16 m, and the transverse direction is divided into two blocks of A and B areas according to the left and right lines, the vertical single layer are no more than 2 m, and the excavation depth of adjacent sections is no more than 2 m. The excavation is longitudinally segmented from the middle of the foundation pit to the east and west ends, and the segment length is not more than 16 m. Strict displacement monitoring is carried out for the subway tunnel passing through it. The possible risks in the project are shown in Table 1.

4.2. Existing Line 5 Guangxi University Station-Xiuling Road Station Tunnel Section. The tunnel line between Guangxi University Station and Xiuling Road Station of Nanning City Line 5 is laid along Ming Xiu Road and crosses the pedestrian bridge of Guangxi Finance and Economics College into Xiuling Road Station, the length of the left line of the interval is 1263.597 m, the length of the right line is 1261.266 m, the total length is 2524.863 m. The tunnels in

this section are buried at a depth of about 9.71–18.72 m and mainly pass through round gravel layers, pebble layers, and silty sand layers. The inner diameter of the shield tunnel in this project is 5400 mm, the thickness of the lining segment is 300 mm, the strength grade is C50, and the impermeability grade is P12. The section is located directly below the underground space engineering project. During the construction of the foundation pit of the project, the shield section is in the state of completion of track laying (not officially in operation).

4.3. Data Collection and Time Window Settings

4.3.1. Data Collection. The initial data of the underground space utilization deep foundation pit project of Nanning Rail Transit Line 5 from Guangxi University Station to Guangxi University of Finance and Economics comes from the monitoring data of the surface settlement and deformation monitoring points and the monitoring data of the tunnel monitoring deformation. Due to a large number of monitoring points, this study only selects some of the monitoring points and monitoring items for analysis. A total of 547 settlement and deformation monitoring points are arranged in and around the deep foundation pit, including surface settlement (408), building settlement (62), and column settlement (85). The type, quantity, and arrangement of monitoring points are shown in Figure 5.

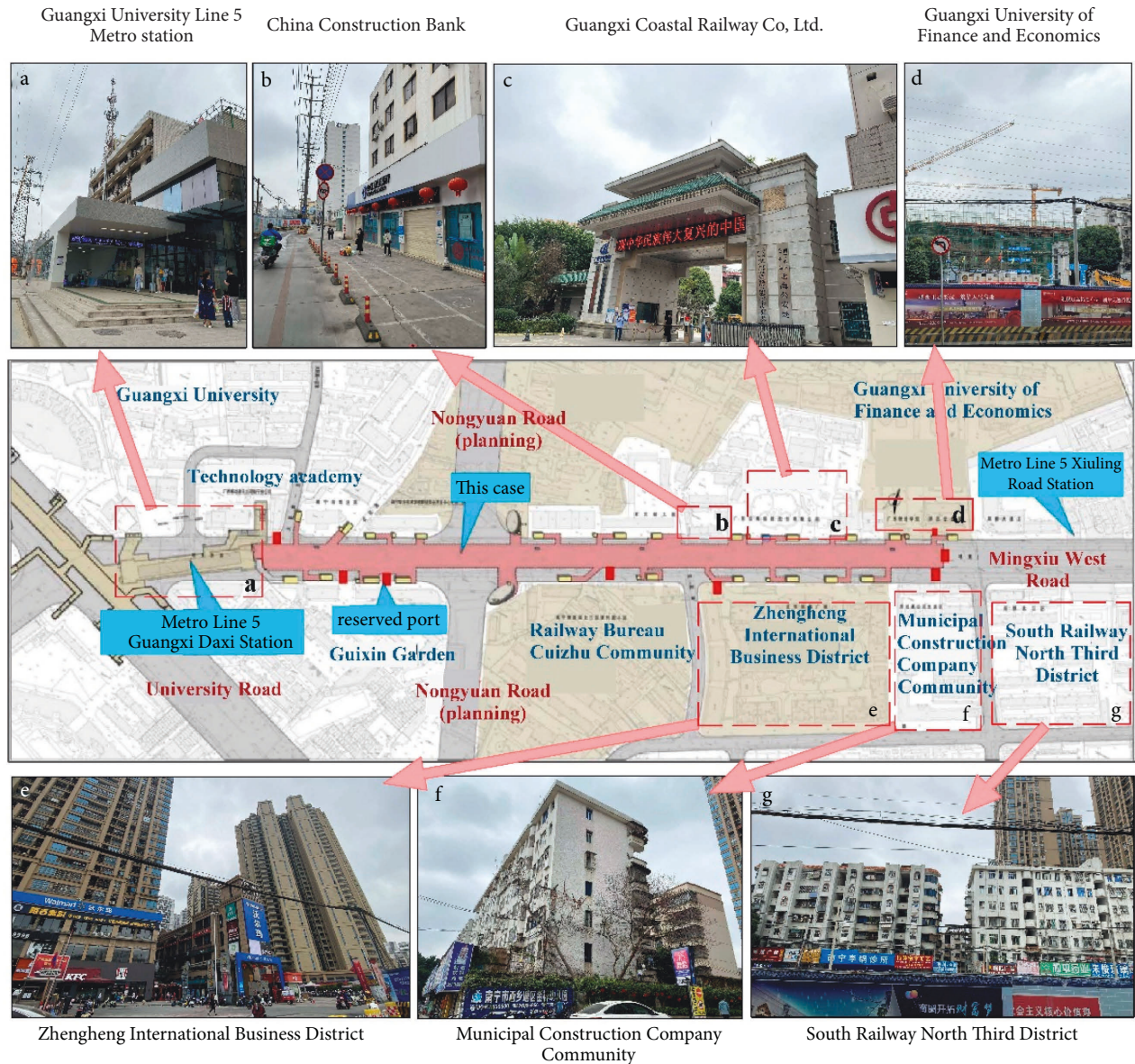


FIGURE 3: The surrounding buildings and environment of the underground project of Guangxi University of Finance and Economics.

During the whole construction process, the structural deformation of the track and subway section is monitored, and automatic detection methods are used for the deformation. The monitoring items include (i) Vertical and lateral deformation monitoring of the tunnel structure and track, (ii) Tunnel structure convergence monitoring, and (iii) For existing Vertical and Lateral Deformation Monitoring of Main and Auxiliary Structures of Subway Stations. In this study, three types of displacement data were selected for analysis: tunnel vertical displacement (102), track vertical displacement (102), and vault settlement (102). The distribution of existing tunnel monitoring points is shown in Figure 6.

4.3.2. *Time Window Division.* For time series, how to transform the time series data at different times into a complex network system model reflecting the current construction process, and how to realize the dynamic evolution of the model with the construction process are the focus of the research. In this study, a moving time observation window is set up on the time axis, and the time series data are divided by the time observation window. The time series in each time observation window generates the complex network model of the deep foundation pit settlement system of the current time window, so as to realize the deep foundation pit. The surface settlement system is constantly changing with the construction process. A fixed-length time observation window

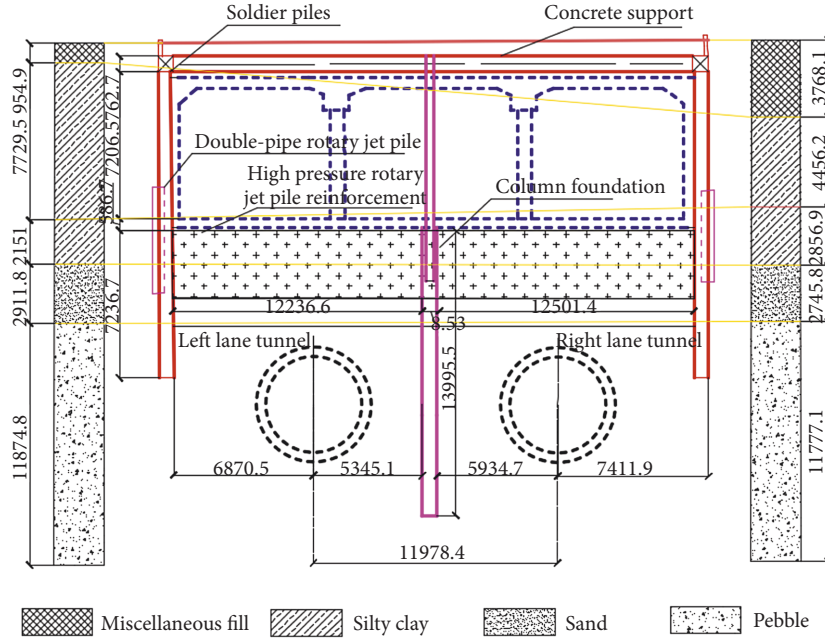


FIGURE 4: Geological section of envelop enclosure.

TABLE 1: The possible risks and their levels in the project.

Risk classification	Location range	Risk description	Risk level
Project's own risk	Open-cut foundation pit	Water gushing and quicksand may occur	III
Environmental risk	Subway tunnel	May cause the tunnel structure to float up and deform, crack and leak water	II
Environmental risk	High voltage line towers and poles	May cause the line tower to settle, tilt	III
Environmental risk	Construction around the foundation pit	May cause house settlement, cracking	III
Environmental risk	Excavation side pipeline	May cause pipeline settlement or leakage	III

$T_1 - T_0$ is set up, and the equidistant translation is performed on the time axis. There are overlapping parts between different windows to ensure the continuity of information in the window. The risk quantification of the complex network model in each window can realize the dynamic evolution research of the construction system of deep foundation pits adjacent to existing tunnels.

Figure 7 shows the time window division of a series of time series data measured at the monitoring points of the deep foundation pit adjacent to the existing subway during the whole construction process. According to its length, time window, and network modeling data volume requirements, it can be divided into several time windows. Figure 7 shows that each monitoring point measured 161-time series data in the 161-day monitoring days. The descriptive statistics of this time series for some monitoring sites are shown in Table 2. The construction process is divided into 20-time windows according to the panning of the windows. The length of the data time window is 30 data, and the length of the time window is an equidistant translation of 7, that is, a time length of 30 days. The amount of shared data in the two windows before and after is 23, that is, the length of time is

23 days. In each time window, a static model of the soil displacement system of the deep foundation pits adjacent to existing tunnels is constructed.

The starting date of the monitoring time series data of this site is September 22, 2021, and the corresponding construction stage is the start of pouring of the crown beam and the production of axes 79–81 concrete supports. The monitoring end date is March 4, 2022, and the corresponding construction stage is grading on the north side of axes 58–59; the second layer of earthwork is excavated on axes 59–61; the roof slab of axes 61–97 has been poured and is being back-filled; axes 97–99 is set up with roof scaffolding; axes 99–100 is used to bind steel bars on the bottom plate; axes 100–102 is used to excavate the second layer of earthwork.

4.4. Construction of the Displacement System Model of the Deep Foundation Pit Adjacent to the Existing Tunnel

4.4.1. Complex Networks under the Time Window. Some related studies [23] have shown that the Pearson coefficient cannot effectively represent the correlation between

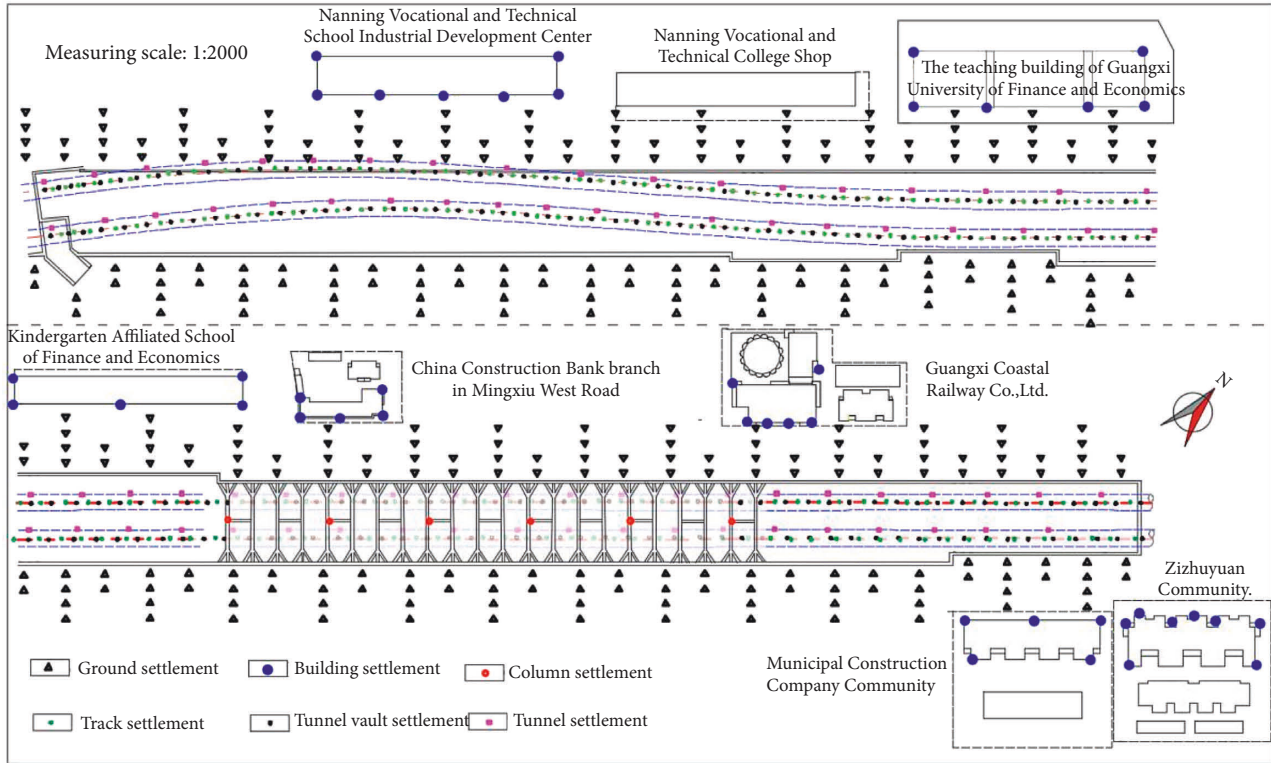


FIGURE 5: Layout of monitoring points.

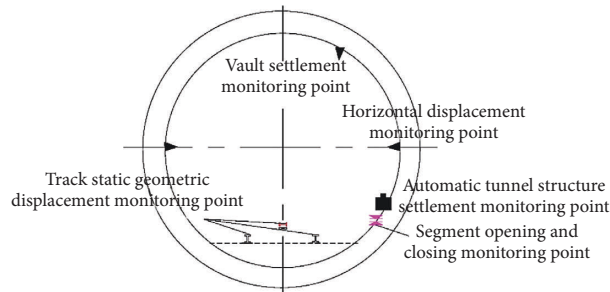


FIGURE 6: Layout of monitoring points of existing tunnel.

nonstationary series. Therefore, this study attempts to use the cross-correlation statistic $Q_{cc}(m)$ to qualitatively analyze whether two-time series have cross-correlation, and calculate the DCCA coefficient to further verify the nonlinear cross-correlation between the data. However, the DCCA coefficient will be affected by the time scale s to varying degrees. The MF-DCCA method for long-range cross-correlation can effectively eliminate the influence of local trends on the time series scale. The Hurst index $H_{xy}(2)$ can be used to further determine the correlation between time series data. The specific solution steps are shown in Figure 8.

Since the construction of the network model is repetitive work, only time window 12 is taken as an example. This time window recorded subsidence data from 861 monitoring points from December 8, 2021, to January 7, 2022, for a total duration of 30 days. According to Section 2.2, the Hurst coefficient describes the correlation between any two nonstationary displacement time series $H_{xy}(2)$.

Using the time-series monitoring data of some monitoring points, calculate the cross-correlation statistics between them according to formula (7). Figure 9 shows the cross-correlation statistics $Q_{cc}(m)$ between D62-2, D63-2, D64-2, J9-1, J9-2, Zlzc-63, Z63, Y63, L63, R63, and D61-2. Where a solid red line represents the chi-square distribution at the 5% significance level, and the degree of freedom m is between 0 and 29. The value of the cross-correlation statistic $Q_{cc}(m)$ between these ten sets of time series data and monitoring point D61-2 time series data exceeds the critical value (chi-square distribution at the 5% significance level), indicating that the null hypothesis that there is no cross-correlation between monitoring point D61-2 and the 10 monitoring points' time series data is rejected at the 5% significance level. This indicates that there is a significant cross-correlation between D61-2 and the ten sets of time series data. To further verify the existence of nonlinear cross-correlation between monitoring point D61-2 and ten sets of time series data, we also calculated DCCA coefficients.

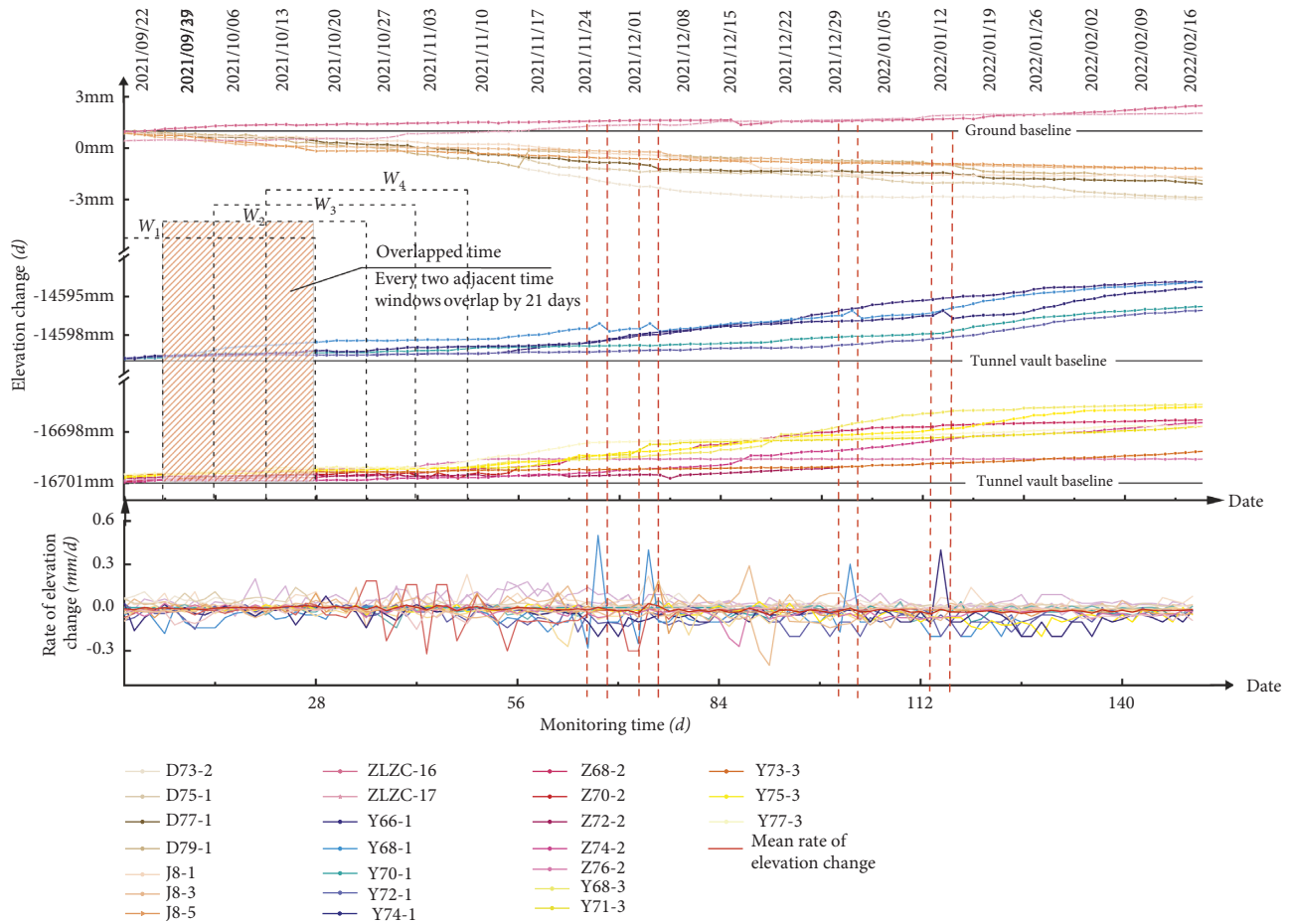


FIGURE 7: Time series and window division of some monitoring points.

According to different scale sizes ($s=2, 4, \text{ and } 8$), different cross-correlation coefficients were calculated (see Table 3). It can be seen from Table 3 that all DCCA coefficients are not equal to 0, indicating that there is a correlation between D61-2 and ten sets of time series data, which is consistent with the previous analysis results of cross statistics.

The cross-correlation statistics $Q_{cc}(m)$ and cross-correlation coefficients only qualitatively detect the nonlinear cross-correlation between D61-2 and ten sets of time series data. Next, we observed nonlinear cross-correlation based on MF-DCCA quantitative research.

The generalized Hurst exponent is calculated according to formulas (9)–(15), and the results are shown in Table 4, and plotted as in Figure 9. It can be seen from Figure 9 that in the short term, the generalized Hurst exponent between D61-2 and ten sets of time series data are not constant, and decreases nonlinearly with the increase of q . When $q=2$, the Hurst index between D61-2 and D63-2 is 0.4815, and the Hurst index between D61-2 and J9-1 is 0.4312, which has a weaker negative long-range correlation. The Hurst exponents of D61-2 and the other eight monitoring time series data are all greater than 0.5, indicating a positive long-range correlation between them. The Hurst index $H_{xy}(2)$ can be used to assess the correlation between time series data. To

this end, the coefficient $H = 2H_{xy}(2) - 1$ can be constructed as the correlation coefficient of any two series X and Y to form the original correlation matrix ($-1 \leq H \leq 1$) between the time series. When H is greater than 0, it means that the two columns of time series data have long-range correlation, when H is less than 0, it means that the two columns of time series data have negative long-range correlation, and when H is equal to 0, it means that the two columns of time series data do not have any correlation.

A complex network can be constructed based on the correlation coefficient matrix. However, if the original correlation coefficient matrix is used as the complex network model, there will be edge connections between any two monitoring points, which leads to an overly complex network model, which is not conducive to extracting the topology parameters of the complex network model. Therefore, the threshold method is needed to streamline and optimize the network, reduce the redundant information in the network, and form a model of the displacement system of the deep foundation pits adjacent to existing tunnels that conforms to the assumption of the nature of the complex network model. To find the optimal threshold, it is necessary to determine the upper and lower limits of the optimal threshold. The specific steps are shown in Figure 8. The

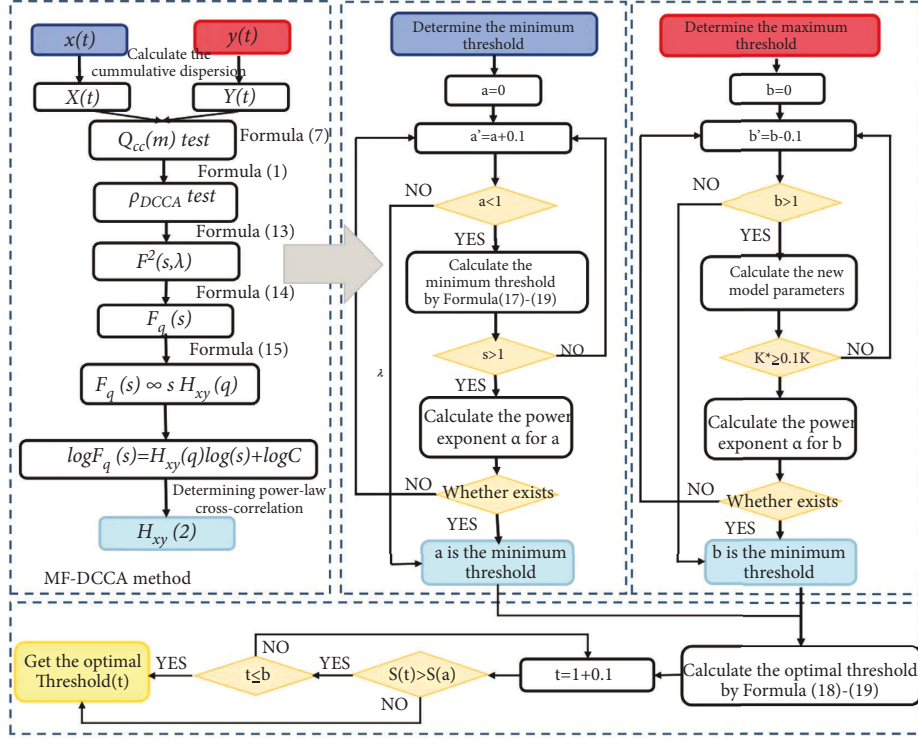


FIGURE 8: Flowchart of Hurst coefficient and optimal threshold determination.

TABLE 2: Descriptive statistics of time series of some monitoring points.

	D62-2	D63-2	D64-2	J9-1	J9-2	Zlzc-63	Z63	Y63	L63	R63	D61-2
Average value	-2.446	-2.556	-2.540	-1.931	-1.926	4.292	3.096	2.709	3.404	2.455	-2.359
Minimum	-2.98	-3.16	-3.84	-2.91	-2.75	3.21	2.54	1.85	2.61	1.79	-3.05
Maximum	-1.95	-2.01	-1.84	-1.43	-1.07	6.28	3.84	3.23	3.87	3.18	-1.77
Standard deviation	0.325	0.383	0.656	0.526	0.597	0.983	0.462	0.447	0.368	0.438	0.390
Skewness	-1.067	-1.337	-0.586	-0.867	-1.465	-0.670	-1.314	-0.949	-0.957	-1.226	-1.137
Peakedness	-0.107	-0.265	-0.924	-0.843	-0.029	0.787	0.504	-0.518	-0.419	0.022	-0.310

threshold values are taken from 1 to 0 in the order of 0.1, and the correlation coefficients are filtered and formed into a new network model based on these thresholds. If when the upper limit of the threshold is b , $K^* \geq 0.1K$ is satisfied, where K is the total number of edges in the existing network and K^* is the total number of edges in the original fully connected network, and the power exponent α exists at this time (according to formula (16)), then b is the upper limit of the threshold. The threshold value is taken from the upper limit b to 0. It takes 0.1 as a unit to calculate the newly formed model parameters, and calculate the small-world index according to formulas (17)–(18). If there is $S > 1$ when the threshold is a , and the power exponent α exists at this time, then determine a as the lower limit of the threshold. Finally, from the upper limit b to the lower limit a , the threshold value takes 0.1 as a unit to calculate the small-world index S of the newly formed model parameters, and the threshold value q when S is the largest is determined as the optimal threshold value, where q satisfies $0 \leq a \leq q \leq b \leq 1$, and the optimal threshold for each time window is shown in Table 5.

The total number of edges in the network is 391755, the average degree $k = 910$, and the threshold method is used to optimize the correlation matrix between time series. For the correlation coefficient H in the original correlation matrix, if it satisfies $|H| < q$, then let $|H| = 0$, if it satisfies $|H| \geq q$, let $|H| = 1$, construct a complex network 0–1 correlation matrix.

According to the abovementioned method, the optimized adjacency matrix graph and the optimized complex network model graph of each time window can be obtained. The complex network model formed by each time window visualizes the relationship and mutual influence of the measurement points of the deep foundation pits adjacent to existing tunnel pits under the time window and the corresponding construction process. Only some window-optimized adjacency matrix graphs and complex network model graphs are shown here. Different colors represent different clusters. Some nodes are distributed on the edge of the complex network graph due to their small degrees, but they are not isolated nodes, as shown in Figure 10.

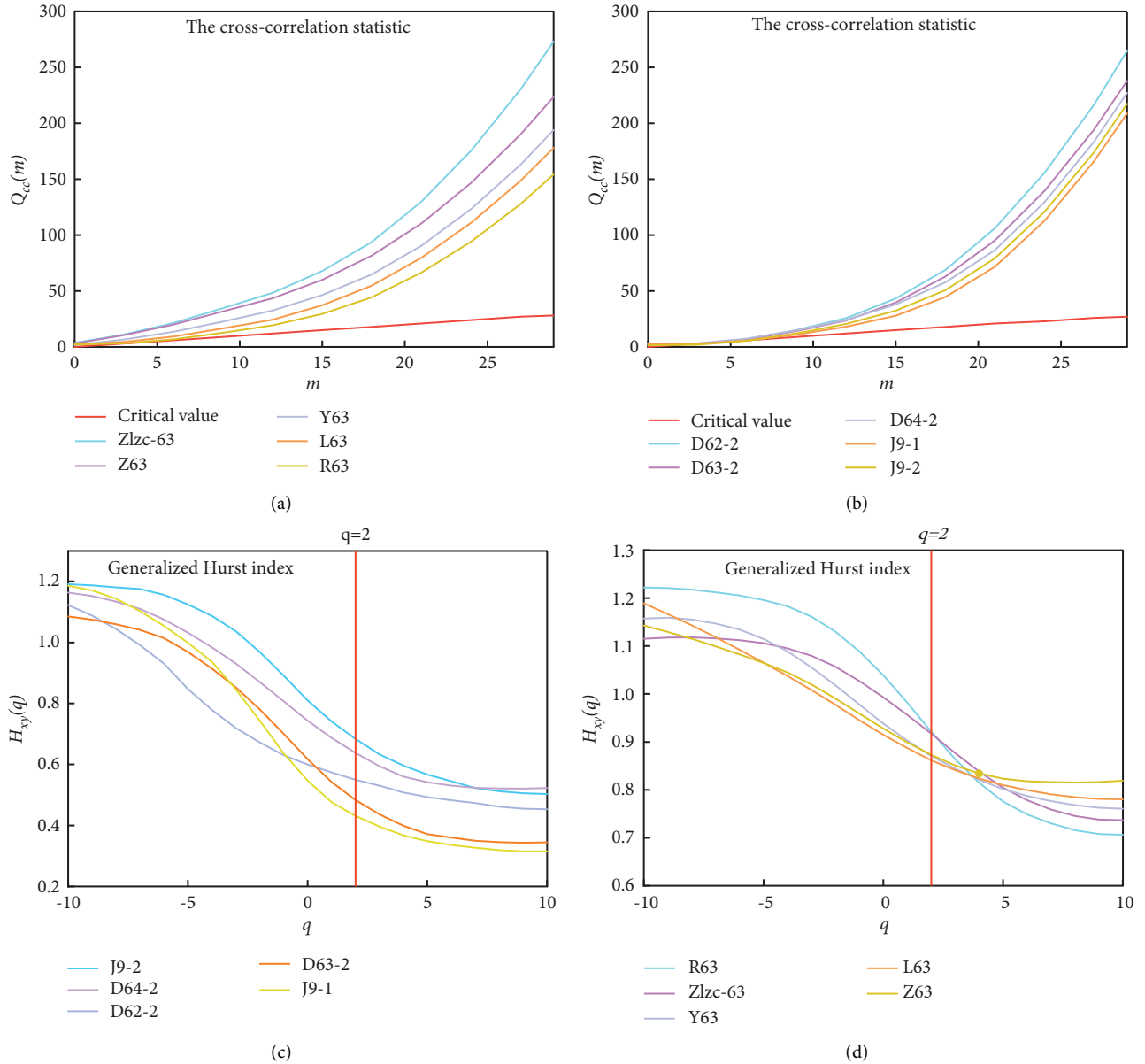


FIGURE 9: Cross-correlation statistic and generalized Hurst exponent between partial time series data.

However, it is impossible to quantitatively assess the overall risk of the deep foundation pit system in adjacent existing tunnels only from the perspective of model visualization. It is also necessary to quantitatively assess the risk distribution and evolution of the deep foundation pit system from the perspective of time and space.

4.4.2. Network Entropy and Structure Evolution. For the system model of the deep foundation pit adjacent to the tunnels, relevant methods and indicators are needed to quantify the size and spatial distribution of the risk level of the foundation pit settlement system reflected by the model. Based on the topological parameters of the complex network model in Section 2.4, from the perspectives of space and time of the deep foundation pit adjacent to the existing tunnel

system, the risk's spatiotemporal distribution assessment and evolution are studied.

From the macroscopic perspective of time, the adjacent system risk value is constructed as an assessment index to measure the risk evolution of the deep foundation pit system network model at different times. The network model of the deep foundation pit network adjacent to the existing tunnel is optimized by the same standard threshold method in all time windows, and the Wu structure entropy and relative risk value \bar{R} are calculated according to formulas (20)–(21), respectively.

The risk threshold of each construction stage is set according to the experience of experts, and the results show that there are four high-risk time periods in the whole process of the foundation pit construction, as shown in Table 5. The evolution and high-risk period of its complex

TABLE 3: DCCA coefficients corresponding to different scales (s).

Time scale (s)	2	4	8
D61-2 and D62-2	0.6914	0.6851	0.6791
D61-2 and D63-2	-0.2145	-0.2098	-0.1899
D61-2 and D64-2	0.7017	0.7329	0.6973
D61-2 and J9-1	-0.3541	-0.3566	-0.3582
D61-2 and J9-2	0.5851	0.5294	0.5327
D61-2 and Zlzc-63	0.7422	0.7216	0.7102
D61-2 and Z63	0.5874	0.5746	0.5784
D61-2 and Y63	0.7234	0.7212	0.7124
D61-2 and L63	0.6912	0.6901	0.6824
D61-2 and R63	0.7147	0.7034	0.7198

TABLE 4: Generalized Hurst index.

q	D62-2	D63-2	D64-2	J9-1	J9-2	Zlzc-63	Z-63	Y63	L63	R63
-10	1.1221	1.0866	1.1634	1.1871	1.1930	1.1156	1.1428	1.1601	1.1886	1.2220
-9	1.0924	1.0717	1.1515	1.1663	1.1840	1.1182	1.1293	1.1553	1.1664	1.2221
-8	1.0331	1.0597	1.1336	1.1455	1.1780	1.1159	1.1159	1.1554	1.1455	1.2172
-7	1.0004	1.0418	1.1098	1.1039	1.1778	1.1185	1.0987	1.1457	1.1185	1.2100
-6	0.9263	1.0121	1.0771	1.0505	1.1569	1.1099	1.0815	1.1359	1.0914	1.2052
-5	0.8522	0.9734	1.0296	1.0030	1.1213	1.1064	1.0656	1.1150	1.0643	1.1979
-4	0.7693	0.9083	0.9851	0.9319	1.0886	1.0954	1.0447	1.0879	1.0385	1.1819
-3	0.7277	0.8549	0.9318	0.8549	1.0382	1.0806	1.0213	1.0571	1.0102	1.1598
-2	0.6684	0.7838	0.8695	0.7364	0.9671	1.0573	0.9917	1.0177	0.9757	1.1339
-1	0.6298	0.6949	0.8072	0.6417	0.8930	1.0277	0.9573	0.9783	0.9461	1.0883
0	0.6031	0.6238	0.7450	0.5439	0.8100	0.9932	0.9277	0.9388	0.9153	1.0402
1	0.5704	0.5378	0.6827	0.4758	0.7360	0.9526	0.8994	0.9006	0.8858	0.9798
2	0.5525	0.4815	0.6412	0.4312	0.6885	0.9218	0.8736	0.8711	0.8624	0.9243
3	0.5287	0.4429	0.5937	0.3986	0.6322	0.8774	0.8502	0.8452	0.8403	0.8638
4	0.5108	0.3925	0.5581	0.3659	0.5906	0.8367	0.8330	0.8194	0.8231	0.8095
5	0.4899	0.3746	0.5431	0.3480	0.5756	0.8022	0.8233	0.8035	0.8121	0.7787
6	0.4838	0.3596	0.5311	0.3389	0.5370	0.7789	0.8185	0.7851	0.7974	0.7467
7	0.4748	0.3506	0.5221	0.3240	0.5280	0.7617	0.8161	0.7765	0.7914	0.7308
8	0.4599	0.3446	0.5219	0.3209	0.5101	0.7433	0.8162	0.7705	0.7853	0.7186
9	0.4538	0.3444	0.5218	0.3148	0.5041	0.7373	0.8176	0.7607	0.7805	0.7063
10	0.4538	0.3444	0.5218	0.3148	0.5041	0.7373	0.8176	0.7607	0.7805	0.7063

network system model in the divided 20-time windows are shown in Figure 11.

From the perspective of the space microcosm, the risk of each monitoring point in the deep foundation pit adjacent system is quantified with betweenness centrality according to formulas (22)–(23). The risk quantification results $R(x_i)$ of each monitoring point are obtained. Based on the magnitude, the monitoring points and calculation results of the high risk in the plane (window 12) and profile (73 axes) of the adjacent existing tunnel deep foundation pit system are shown in Tables 6 and 7. The risk distribution assessment map of the deep foundation pit construction system is formed, and the high-risk parts in the foundation pit construction are warned.

5. Verification and Discussion

5.1. Effectiveness Analysis of High-Risk Period Warnings. The assessment method in this study is to quantify the overall risk through the interaction between monitoring

points in deep foundation pit construction and the impact on the overall system because different construction stages will be affected by different environmental conditions, so dynamic risk thresholds are set based on expert experience, and there are four high-risk windows. They are window 6 (2021.10.12–11.26), window 12 (2021.12.8–2022.1.7), window 13 (2021.12.15–2022.1.14), and window 18 (2022.1.19–2.18). Through the “Weekly Security Inspection Report,” it was found that there were three dangerous on-site incidents recorded in the project from the start of construction to the present. It is just divided into corresponding window 12, window 13, and window 18, indicating that the method in this study can achieve effective early warning in time, as shown in Table 8.

However, the traditional method of using the threshold method is based on the data of a single monitoring point for early warning. The number of times effective early warning is only one time (accident 2). The traditional method has appeared in judging experience and data observation of a single monitoring point. Missing and misjudging risks,

TABLE 5: Optimal thresholds and complex network features for each time window.

Date	Lower threshold	Upper threshold	Optimal threshold	Features of the complex network under the optimal threshold			E	Risk value
				K^*	k	s		
				\bar{R}				
2021.09.22–10.22	0.2	0.7	0.7	130553	303.26	1.478	5.06810061	0.465
09.29–10.29	0.1	0.5	0.4	277031	643.51	1.157	5.080694814	0.591
10.06–11.05	0.2	0.4	0.4	285288	662.69	1.105	5.073498126	0.519
10.13–11.12	0.3	0.5	0.5	196803	457.15	1.234	5.07709647	0.555
10.20–11.19	0.3	0.5	0.5	319104	741.24	1.184	5.089390812	0.678
10.27–11.26	0.2	0.5	0.5	235143	546.21	1.224	5.09458842	0.73
11.03–12.03	0.3	0.6	0.6	181421	421.42	1.319	5.081894262	0.603
11.10–12.10	0.2	0.7	0.5	220907	513.14	1.286	5.021622	0
11.17–12.17	0.1	0.3	0.3	335855	780.15	1.131	5.073198264	0.516
11.24–12.24	0.2	0.5	0.4	319061	741.14	1.129	5.056405992	0.348
12.01–12.31	0.1	0.5	0.4	267431	621.21	1.183	5.079795228	0.582
12.08–2022.1.7	0.2	0.5	0.5	190341	442.14	1.209	5.121576	1
12.15–01.14	0.3	0.7	0.6	194862	452.64	1.313	5.07859578	0.57
12.22–01.21	0.2	0.6	0.5	194646	452.14	1.264	5.073797988	0.522
12.29–01.28	0.1	0.6	0.6	189222	439.54	1.373	5.069000196	0.474
2022.1.5–2.04	0.1	0.5	0.5	204277	474.51	1.198	5.071698954	0.501
1.12–2.11	0.2	0.6	0.5	244313	567.51	1.171	5.078895642	0.573
1.19–2.18	0.1	0.4	0.4	298832	694.15	1.137	5.08559256	0.64
1.26–2.25	0.1	0.6	0.4	293661	682.14	1.119	5.081294538	0.597
2.02–3.04	0.2	0.5	0.5	215181	499.84	1.229	5.079795228	0.582

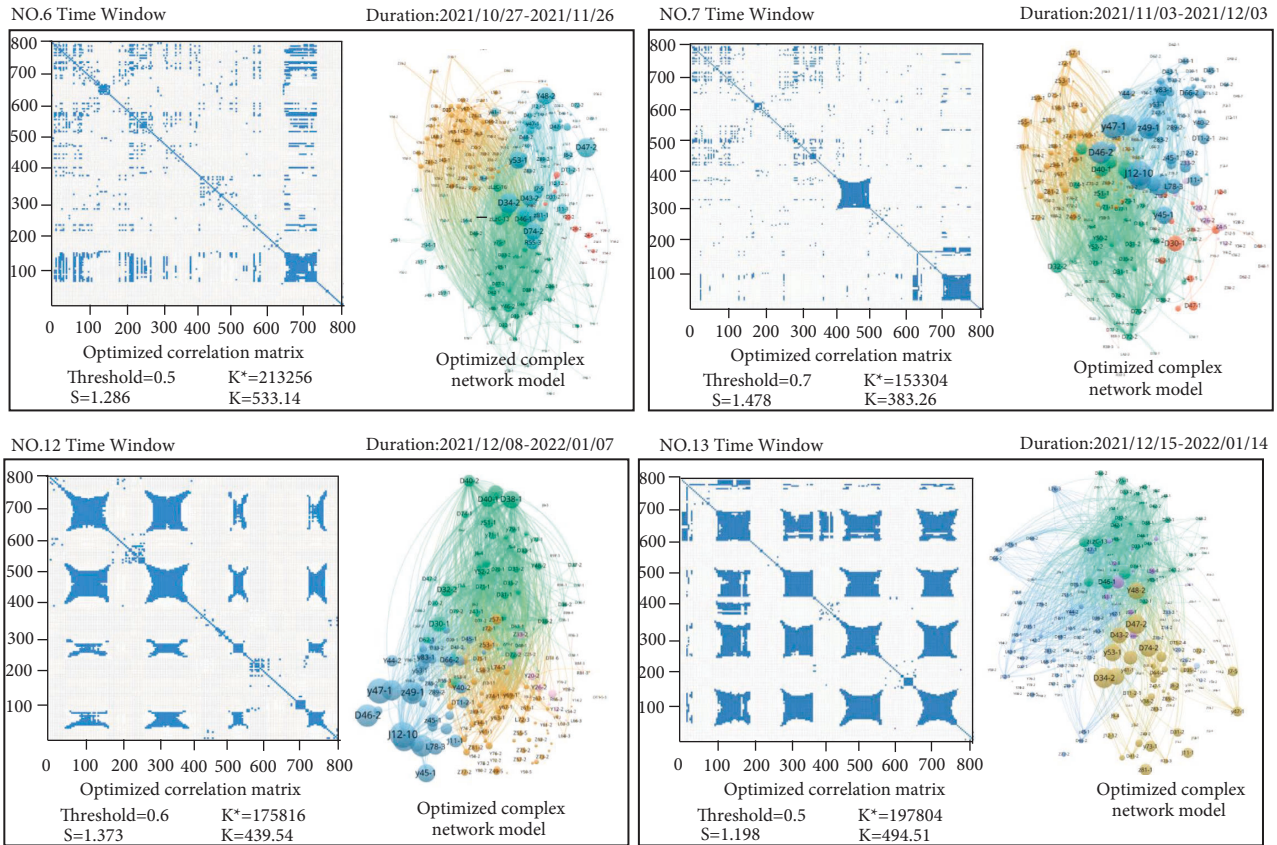


FIGURE 10: Complex network model of the partial time window during construction of deep foundation pit adjacent to tunnels.

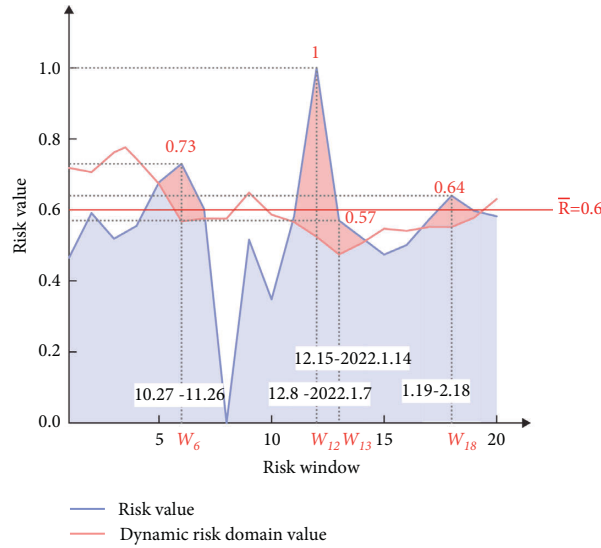


FIGURE 11: Risk evolution diagram of settlement system during the whole construction process of deep foundation pit adjacent to existing subway.

TABLE 6: Betweenness centrality of each monitoring point in the 73-axis profile.

Order	Monitoring	Settlement value	Betweenness	$R(x_i)$
1	D73-2	-5.35	0.0140	1
2	D73-1	-3.05	0.0108	0.768
3	Z73	3.67	0.0034	0.243
4	L73	3.24	0.0033	0.238
5	Z73	2.84	0.0030	0.216
6	Zlzc-62	6.28	0.0026	0.184
7	D73-3	-2.12	0.0024	0.172
8	R73	2.14	0.0023	0.165
9	Y73	2.31	0.0020	0.143
10	D73-4	-3.84	0.0020	0.140
11	Y73	1.98	0.0019	0.134

leading to unforeseen first and third accidents. Taking the first accident as an example, when the danger of leakage occurred, the constructor immediately shot the anchor. However, a small amount of stagnant water in the upper layer still seeped out from the surface of the shotcrete. From the data of a single monitoring point, D73-2 (-5.35 mm), D73-1 (-3.05 mm), Z73 (3.47 mm), z73 (4.08 mm), L73 (3.98 mm) are far from the risk domain value both in terms of cumulative settlement and single day increase, which is also an important reason for the warning failure. However, the new method of this study has an early warning (window 6) and no risk event was found. It is speculated that the reason is that the bottom sealing speed of the bottom plate during the construction of the axes 79–81 is faster, which avoids soil disturbance and avoids the occurrence of dangerous situations to a certain extent. From the perspective of time, the new assessment method can more effectively warn the high-risk period than the traditional method, and enhance the safety management ability of deep foundation pit construction in terms of early warning. The reasons for the defects of the traditional method are: (1) It is difficult to

judge the overall risk of the system from a single monitoring point and engineering experience, and there is a lack of in-depth research on the mechanism of dangerous situations. (2) The system is nonlinear, and the evolution law of risk is not linear. Levels increase significantly beyond a threshold at a certain point in time, causing a sudden onset of a near-miss event.

5.2. Analysis of the Accuracy of Prediction of High-Risk Parts.

It is not enough to predict dangerous situations only in time. The ability to accurately predict the specific location of the risk from space is essential for accurate early warning of dangerous situations. This study quantifies the risk of each monitoring point in the deep foundation pit system and describes the distribution of the risk of the project in both plan and profile based on the values of each monitoring point.

The first dangerous event in deep foundation pit construction occurred on January 2, 2022, in the axes 73–76 construction interval in the foundation pit. The plan view and cross-sectional view of the risk distribution assessment corresponding to window 12 are shown in Figures 12 (a) and 12 (b). The axes 73–76 axis in the risk assessment plan show that the risk value is higher, and the risk maximum value is reached at the axes 73 ($R(D73-2) = 1$). In the sectional view, the predicted location of the accident is the surface of the monitoring point D73-2 on the north side of the axes 73, which is very close to the location of the accident. Figure 12(c) shows a schematic diagram of the construction situation and the surrounding environment when the danger occurs. According to the “Special Report on Safety Accidents,” the scope of the dangerous situation is the north side of the perimeter pile of axis 73–76, there are signs of water seepage between the retaining piles, and the pit pumping machine immediately pumped water and sprayed anchor

TABLE 7: Top 59 high-risk monitoring points based on betweenness centrality.

Order	Monitoring points	Settlement value	Betweenness	$R(x_i)$
1	D73-2	-5.35	0.0140	1
2	D72-2	-5.21	0.0132	0.942
3	D74-2	-2.86	0.0120	0.854
4	D76-2	-5.14	0.0117	0.834
5	D66-2	-2.21	0.0109	0.774
6	D73-1	-3.05	0.0108	0.768
7	D74-1	-1.84	0.0105	0.751
8	D75-2	-2.51	0.0104	0.744
9	D75-1	-1.74	0.0102	0.731
10	D66-1	-0.26	0.0100	0.712
11	D65-2	-1.08	0.0098	0.698
12	D67-2	-0.43	0.0097	0.694
13	D76-1	-2.34	0.0097	0.691
14	D72-1	-1.15	0.0096	0.686
15	D67-1	-3.14	0.0096	0.684
16	D65-1	-1.95	0.0096	0.683
17	D64-2	-4.54	0.0095	0.674
18	D76-2	-3.36	0.0093	0.661
19	D76-1	-3.87	0.0091	0.651
20	D71-2	-2.73	0.0091	0.651
21	D61-2	-4.19	0.0090	0.644
22	D64-2	-3.84	0.0090	0.642
23	D63-2	-3.16	0.0090	0.641
24	D62-2	-2.98	0.0088	0.631
25	D63-1	-4.95	0.0088	0.629
26	D62-1	-5.17	0.0088	0.628
27	D81-2	-3.18	0.0088	0.625
28	D81-1	-2.84	0.0087	0.624
29	D77-2	-2.16	0.0087	0.622
30	D61-1	-2.47	0.0087	0.620
31	D77-1	-2.42	0.0087	0.619
32	D77-2	-3.21	0.0087	0.617
33	D70-2	-2.81	0.0086	0.615
34	J9-3	-1.63	0.0086	0.615
35	Z67	6.51	0.0086	0.614
36	J9-2	-2.75	0.0086	0.613
37	J9-1	-2.91	0.0086	0.612
38	D80-2	-2.25	0.0086	0.611
39	J9-4	-1.60	0.0086	0.610
40	D68-2	-2.49	0.0085	0.609
41	D69-2	-2.31	0.0085	0.608
42	D68-1	-3.71	0.0085	0.607
43	D69-1	-3.16	0.0085	0.606
44	D60-2	-2.51	0.0085	0.606
45	D60-1	-2.94	0.0085	0.606
46	Z69	4.48	0.0085	0.605
47	Z65	4.34	0.0085	0.604
48	Z63	3.87	0.0084	0.599
49	Z61	2.21	0.0084	0.597
50	D79-1	-3.15	0.0083	0.595
51	D82-1	-2.62	0.0083	0.594
52	D82-2	-2.18	0.0083	0.591
53	D83-1	-2.59	0.0080	0.574
54	D78-1	-3.04	0.0080	0.574
55	D78-2	-3.16	0.0080	0.569
56	D79-1	-3.01	0.0079	0.566
57	D59-2	-2.57	0.0079	0.564
58	D79-2	-3.29	0.0079	0.563
59	D58-2	-2.82	0.0079	0.562
...

TABLE 8: Dangerous events and warnings in the whole process of deep foundation pit construction adjacent to existing tunnels.

Accidents	Time	Accident location	Construction procedures and causes	Whether there is an effective warning	
				Traditional method	This research method
1	2022.1.2	There are signs of water seepage between the piles of axes 73–76, and there are large areas of wet stains	The roof of axes 70–73 is being poured, and the cause of the accident is that the shotcrete anchor of axes 73–76 is backward	No	Yes
2	2022.1.13	There is water gushing in the water collecting well of axes 84, and there is a large amount of ponding at the bottom of the foundation pit	The cushion of axes 83–85 has been poured and is being constructed as a concrete base plate. The second layer of earthwork is excavated on the south side of axes 83–85. The cause of the accident was the increase in rainfall in January and the burst of the sewage pipeline, resulting in a large amount of sewage gushing out	Yes	Yes
3	2022.2.12	There are slight signs of water seepage between the piles of axes 91–95, and there are large areas of wet stains	The bottom plate of zone A of axes 94–95 has been poured; the floor of zone B is being constructed. The cause of leakage is unknown	No	Yes

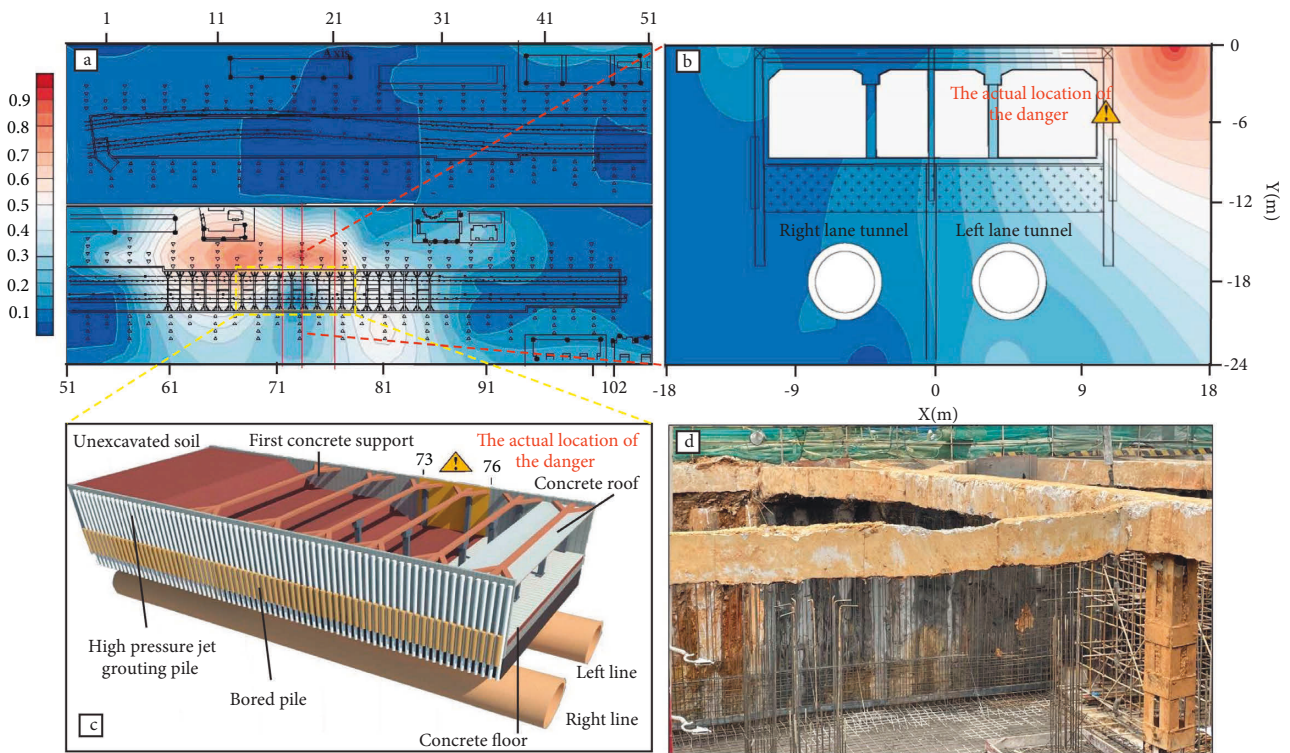


FIGURE 12: Comparative analysis of the first risk assessment and the actual situation: (a) risk distribution assessment plan; (b) risk distribution assessment sectional view; (c) construction status and actual location of the accident at the time of the first accident ; (d) the scene of the first accident.

when the accident occurred. Figure 12(d) shows the site situation when the danger occurs. There are still many water seepage marks on the concrete of the shotcrete. Obviously, the shotcrete is lagging.

The second accident occurred on January 13, 2022, in the 84-axis catchment well. The plan view and cross-sectional view of the risk distribution assessment of the deep

foundation pit corresponding to window 13 are shown in Figures 13 (a) and 13 (b). Risk Plane (Figures 13 (a)) shows a high-risk range on axes 83 to axes 88 with a risk maximum on axes 85 ($R(Y_{85-2}) = 1$). In the 84-axis profile (Figure 13(b)), the places with high-risk values are the vault settlement of the right-line tunnel ($R(\gamma_{84-2}) = 0.86$), the vertical displacement of the right-line tunnel ($R(Y_{84-2})$)

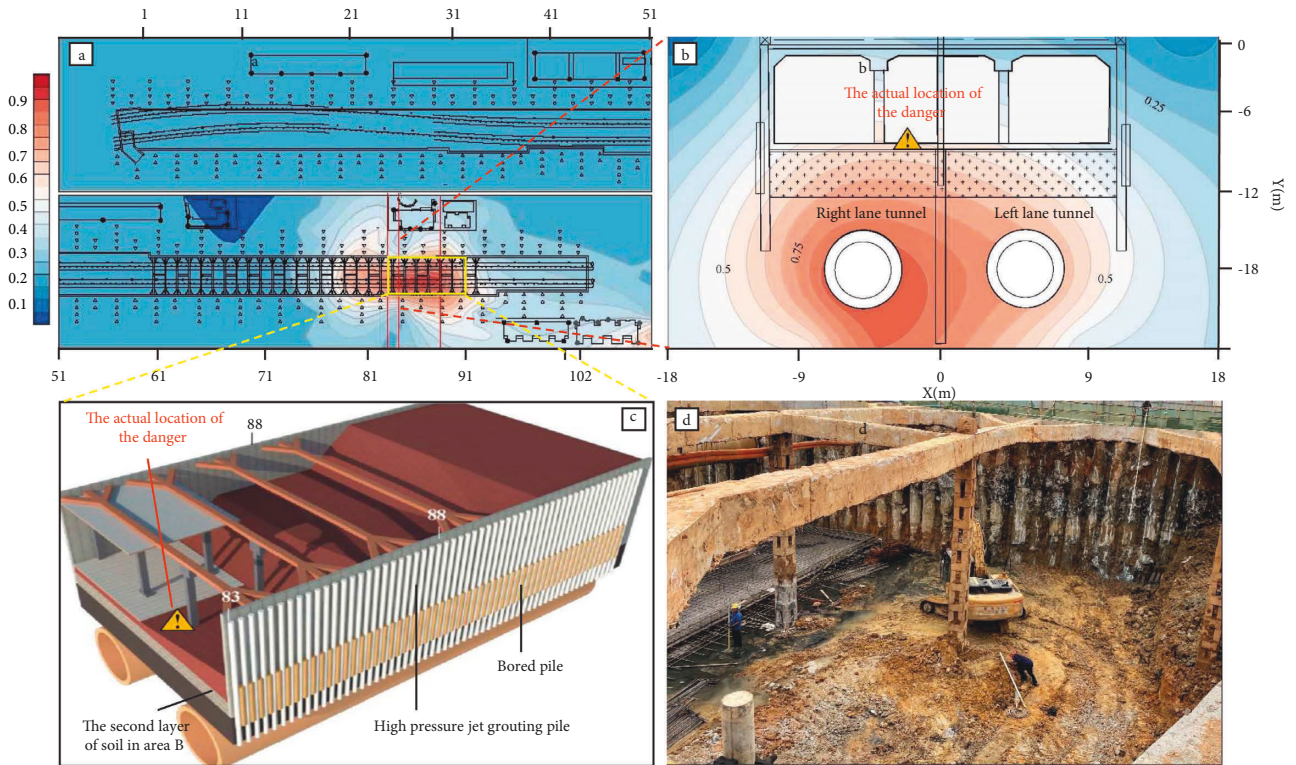


FIGURE 13: Comparative analysis of the second risk assessment and the actual situation: (a) risk distribution assessment plan; (b) risk distribution assessment sectional view; (c) construction status and actual location of the accident at the time of the second accident; (d) the scene of the second accident.

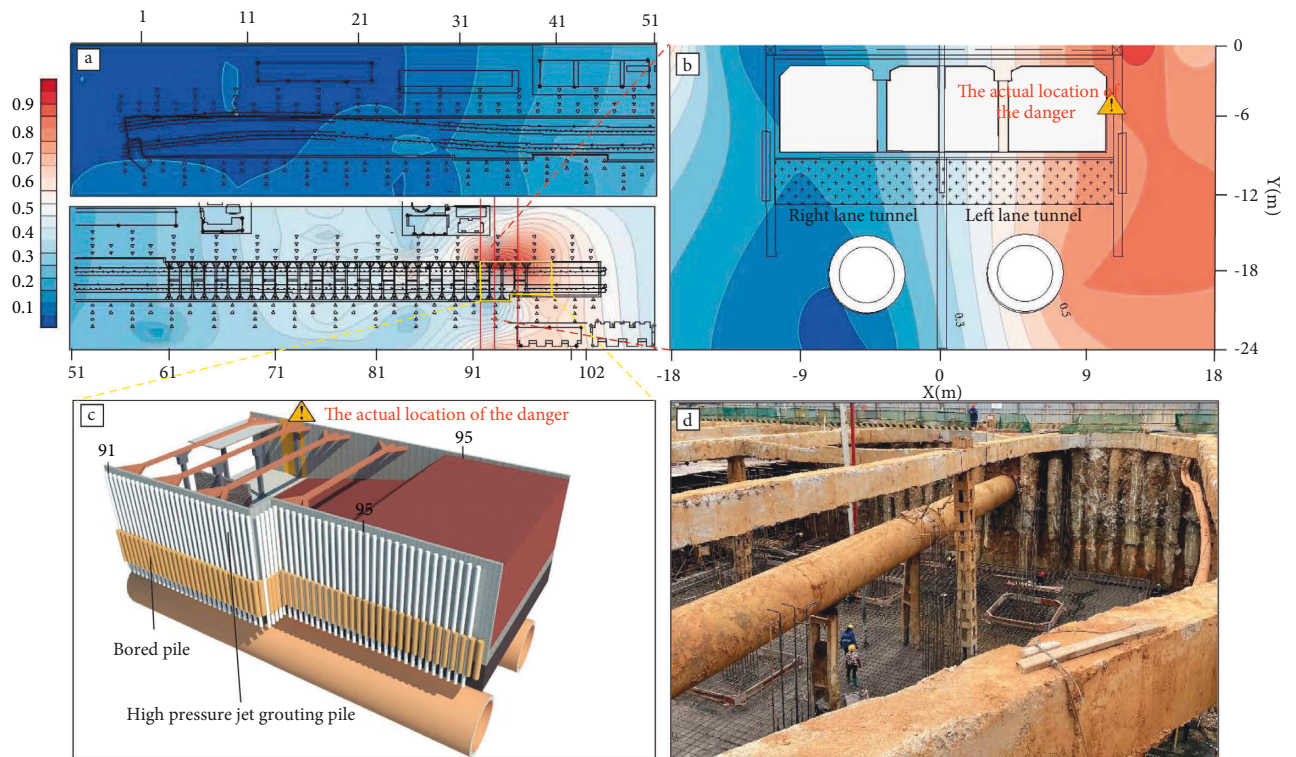


FIGURE 14: Comparative analysis of the third risk assessment and the actual situation: (a) risk distribution assessment plan; (b) risk distribution assessment sectional view; (c) construction status and actual location of the accident at the time of the third accident; (d) the scene of the third accident.

= 0.81), and the vertical displacement of the right-line track ($R(R84-2) = 0.80$). It is not the part where the accident occurred, but it is very close to the part where the accident occurred, and can effectively warn the accident part beforehand. This situation is similar to that of accident 1. It is speculated that the reason is that there is no displacement monitoring point arranged at the location where the danger occurs, so the risk information can only be transmitted through its adjacent monitoring points. Figure 13(c) shows the construction situation and the location where the dangerous situation occurs. According to the “Weekly Security Inspection Report,” there is water gushing in the axes 84 water collecting well, and there is a large amount of water at the bottom of the foundation pit. The builder had filled in small diameter stones at the time of the hazard and filled in dry concrete and micro-expansion concrete. Figure 13(d) shows the scene when the danger occurred. It can be seen that there is a large amount of undischarged sewage at the bottom of the pit. It is speculated that the cause of the accident may be the increase of rainwater at that time, and the rupture of the sewage pipeline near the foundation pit, resulting in drainage. The well is overloaded and fails.

The third accident of the foundation pit occurred on February 12, 2022, in the axes 91–95 construction section. The risk assessment plan of window 18 in Figure 14(a) shows that the high-risk range is in the axes 91–95, and the risk maximum value ($R(D93-2) = 1$) appears in the axes 93, which is consistent with the actual accident site (Figure 14(c)). In the risk evaluation profile (in Figure 14(b)), the monitoring point with the highest risk is also D93-2 and shows that the pile on the north side of axis 93 is a high risk, which is consistent with the actual situation and illustrates the accuracy of the risk evaluation. Figure 14(c) shows the construction situation and the location where the dangerous situation occurs. According to the “Special Report on Safety Accidents,” there is a large area of water seepage between the piles in the construction area of axes 91 to 95 construction area. Vein-like structure formed by high-pressure grouting to seal gaps in cement-reinforced soil and soil. Figure 14(d) shows the on-site situation at the time of the accident. There are signs of water seepage among the piles. The plugging effect is good after the event. It is presumed that it is a natural leakage with little impact on construction safety.

The results of the three accident analyses show that the new assessment method is of great significance for strengthening the safety risk monitoring of the displacement system of deep foundation pits in deep adjacent subways and enhancing the safety management ability of deep foundation pit construction under such complex backgrounds.

6. Conclusion

Based on the complex network theory, this research establishes a complex network model of the displacement system of the deep foundation pit adjacent to the existing tunnel and constructs the risk index to assess the risk of the foundation pit system and the spatial distribution of risk.

Finally, based on the analysis of engineering experience and case studies, the following conclusions are drawn:

This study introduces the MF-DCCA method for the first time to explore the correlation between nonstationary time series data, and uses the threshold method to convert the original correlation matrix into an adjacency matrix. Make an optimized static model of the system of deep foundation pits adjacent to existing tunnels in each time window. Compared with the actual construction situation, the results show that the visual evolution of the complex network model under different windows can reflect the impact of the foundation pit construction process on the system risk of the deep foundation pit adjacent to the existing tunnel. The feasibility of constructing a static risk model of a deep foundation pit adjacent to an existing tunnel is illustrated based on the MF-DCCA method and the threshold method. The transformation from a large amount of unstable time series data to a visible and measurable model is realized, and then the interrelation and overall characteristics of each element in the adjacent existing subway foundation pit system are described.

The overall risk evolution and distribution of the deep foundation pit adjacent to existing tunnels are quantified from the time angle and space. The time and location of the actual risk occurrence are compared and analyzed. The results show that: this method can effectively predict the time and location of the three safety accidents, which is of great engineering significance for strengthening the safety risk monitoring of the adjacent existing subway deep foundation pit displacement system and providing an effective basis for prewarning and risk control.

This research compares the effectiveness and accuracy of this method with the traditional method in terms of the effectiveness and accuracy of warning from the risk period based on the three dangerous events recorded in the actual construction of the case project. The results show that the new assessment method can effectively warn three times. In contrast, the traditional method is only one time, indicating that the new assessment method can more effectively warn the high-risk period than the traditional method from a macro perspective. It can strengthen the safety monitoring and construction safety management of complex engineering displacement systems such as deep foundation pits adjacent to existing subway tunnels.

Data Availability

The data used to support the findings of this study are currently under embargo while the research findings are commercialized. Requests for data, 12 months after publication of this article, will be considered by the corresponding author.

Conflicts of Interest

The authors declare that there are no conflicts of interest regarding the publication of this paper.

Acknowledgments

This research was funded by the National Natural Science Foundation of China (Grant no. 52068004), Natural Science Foundation of Guangxi (Grant no. 2018GXNSFAA050063), and Key Research Projects of Guangxi (Grant no. AB19245018).

References

- [1] A. S. Osman and M. D. Bolton, "Ground movement predictions for braced excavations in undrained clay," *Journal of Geotechnical and Geoenvironmental Engineering*, vol. 132, no. 4, pp. 465–477, 2006.
- [2] Z. Zhang and M. Huang, "Geotechnical influence on existing subway tunnels induced by multiline tunneling in Shanghai soft soil," *Computers and Geotechnics*, vol. 56, pp. 121–132, 2014.
- [3] H.-B. Zhang, J.-J. Chen, X.-S. Zhao, J.-H. Wang, and H. Hu, "Displacement performance and simple prediction for deep excavations supported by contiguous bored pile walls in soft clay," *Journal of Aerospace Engineering*, vol. 28, no. 6, 2015.
- [4] Z. Jiang, *Study of Mechanical Response on Adjacent Tunnel in Processes of Foundation Excavation*, Chongqing University, Chongqing, China, 2013.
- [5] B. Li, Q. f. Ding, N. w. Xu, F. Dai, Y. Xu, and H. I. Qu, "Characteristics of microseismic b-value associated with rock mass large deformation in underground powerhouse caverns at different stress levels," *Journal of Central South University*, vol. 29, no. 2, pp. 693–711, 2022.
- [6] X. P. Lai, M. F. Cai, and M. W. Xie, "In situ monitoring and analysis of rock mass behavior prior to collapse of the main transport roadway in Linglong Gold Mine, China," *International Journal of Rock Mechanics and Mining Sciences*, vol. 43, no. 4, pp. 640–646, 2006.
- [7] G. Zheng, Y. Du, Y. Diao, X. Deng, G. Zhu, and L. Zhang, "Influenced zones for deformation of existing tunnels adjacent to excavations," *Chinese Journal of Geotechnical Engineering*, vol. 38, no. 4, pp. 599–612, 2016.
- [8] Z. Jiang and Y. Zhang, "Calculation of influence on longitudinal deformation of adjacent tunnels due to excavation," *Journal of Civil, Architectural & Environmental Engineering*, vol. 35, no. 1, pp. 7–11, 2013.
- [9] C. Xu, Y. Wang, Y. Xu, and J. Wang, "Effect of foundation pit excavation and structural construction of new engineering on existing underlying tunnel," *Rock and Soil Mechanics*, vol. 36, no. 11, pp. 3201–3209, 2015.
- [10] F. Wang, *Study on the Modelling and Dynamics of Safety Risk during Tunnel Construction*, Huazhong University of Science and Technology, 2013.
- [11] X. Bao, Y. Fu, and H. Huang, "Case study of risk assessment for safe grade of deep excavations," *Chinese Journal of Geotechnical Engineering*, vol. 36, no. S1, pp. 192–197, 2014.
- [12] C. Xu and Q. Ren, "Fuzzy-synthetic evaluation on stability of surrounding rockmasses of underground engineering," *Chinese Journal of Rock Mechanics and Engineering*, vol. 23, no. 11, pp. 1852–1853, 2004.
- [13] W. Ting, W. Liu, C. Zhang, H. He, and X. Li, "Study on ground settlement induced by shallow metro station constructions," *Chinese Journal of Rock Mechanics and Engineering*, vol. 26, no. 9, pp. 1855–1861, 2007.
- [14] C. Y. Ou and P. G. Hsieh, "A simplified method for predicting ground settlement profiles induced by excavation in soft clay," *Computers and Geotechnics*, vol. 38, no. 8, pp. 987–997, 2011.
- [15] M. G. Li, X. Xiao, J. H. Wang, and J. J. Chen, "Numerical study on responses of an existing metro line to staged deep excavations," *Tunnelling and Underground Space Technology*, vol. 85, pp. 268–281, 2019.
- [16] C. Zhou, T. Kong, S. Jiang, S. Chen, Y. Zhou, and L. Ding, "Quantifying the evolution of settlement risk for surrounding environments in underground construction via complex network analysis," *Tunnelling and Underground Space Technology*, vol. 103, Article ID 103490, 2020.
- [17] M. J. Bryn, D. A. Afonin, and N. N. Bogomolova, "Geodetic monitoring of deformation of building surrounding an underground construction," in *International Scientific Conference on Transportation Geotechnics and Geoecology (TGG)* pp. 386–392, Saint Petersburg, RUSSIA, 2017.
- [18] M. E. Alaoui, E. Bouri, and D. Roubaud, "Bitcoin price volume: a multifractal cross-correlation approach," *Finance Research Letters*, vol. 31, pp. 374–381, 2019.
- [19] X. Xiong, K. Xu, and D. Shen, "Dynamic cross-correlations between investors' attention and CSI300 index futures," *Fluctuation and Noise Letters*, vol. 18, no. 04, Article ID 1950022, 2019.
- [20] Y. Cai, X. Lu, Y. Ren, and L. Qu, "Exploring the dynamic relationship between crude oil price and implied volatility indices: a MF-DCCA approach," *Physica A: Statistical Mechanics and its Applications*, vol. 536, Article ID 120973, 2019.
- [21] W. X. Zhou, "Multifractal detrended cross-correlation analysis for two nonstationary signals," *Physical Review*, vol. 77, no. 6, Article ID 066211, 2008.
- [22] R. Vassoler and G. Zebende, "DCCA cross-correlation coefficient apply in time series of air temperature and air relative humidity," *Physica A: Statistical Mechanics and Its Applications*, vol. 391, no. 7, pp. 2438–2443, 2012.
- [23] L. Kristoufek, "Measuring correlations between non-stationary series with DCCA coefficient," *Physica A: Statistical Mechanics and its Applications*, vol. 402, pp. 291–298, 2014.
- [24] G. F. Zebende, "DCCA cross-correlation coefficient: quantifying level of cross-correlation," *Physica A: Statistical Mechanics and its Applications*, vol. 390, no. 4, pp. 614–618, 2011.
- [25] J. W. Kantelhardt, S. A. Zschiegner, E. Koscielny-Bunde, S. Havlin, A. Bunde, and H. E. Stanley, "Multifractal detrended fluctuation analysis of nonstationary time series," *Physica A: Statistical Mechanics and its Applications*, vol. 316, no. 1–4, pp. 87–114, 2002.
- [26] B. Podobnik and H. E. Stanley, "Detrended cross-correlation analysis: a new method for analyzing two nonstationary time series," *Physical Review Letters*, vol. 100, no. 8, Article ID 084102, 2008.
- [27] B. Podobnik, Z. Q. Jiang, W. X. Zhou, and H. E. Stanley, "Statistical tests for power-law cross-correlated processes," *Physical Review*, vol. 84, no. 6, Article ID 066118, 2011.
- [28] R. Albert and A. L. Barabasi, "Statistical mechanics of complex networks," *Reviews of Modern Physics*, vol. 74, no. 1, pp. 47–97, 2002.
- [29] A. L. Barabasi and R. Albert, "Emergence of scaling in random networks," *Science*, vol. 286, no. 5439, pp. 509–512, 1999.
- [30] M. Rubinov, S. A. Knock, C. J. Stam et al., "Small-world properties of nonlinear brain activity in schizophrenia," *Human Brain Mapping*, vol. 30, no. 2, pp. 403–416, 2009.
- [31] Y. Du, *The Study of Identifying Influential Nodes in Complex Networks*, Southwest University, El Paso, Texas, USA, 2015.
- [32] M. Cai, H. Du, Y. Ren, and M. W. Feldman, "A new network structure entropy based node difference and edge difference," *Acta Physica Sinica*, vol. 60, no. 11, Article ID 110513, 2011.

- [33] P. Luo, Y. Li, and C. Wu, "Complex networks evolution research using the network structure entropy," *Complex Systems and Complexity Science*, vol. 10, no. 4, pp. 62–68, 2013.
- [34] Y. Tan and J. Wun, "Network structure entropy and its application to scale-free networks," *Systems Engineering-Theory & Practice*, vol. 24, no. 6, pp. 1–3, 2004.
- [35] K. Berahmand, A. Bouyer, and N. Samadi, "A new centrality measure based on the negative and positive effects of clustering coefficient for identifying influential spreaders in complex networks," *Chaos, Solitons & Fractals*, vol. 110, pp. 41–54, 2018.